IEEE Access
Multidisciplinary | Rapid Review | Open Access Journal

Received December 24, 2020, accepted January 2, 2021, date of publication January 8, 2021, date of current version January 14, 2021.

*Digital Object Identifier 10.1109/ACCESS.2021.3049832*

# Fuzzy Linear Active Disturbance Rejection Control of Injection Hybrid Active Power Filter for Medium and High Voltage Distribution Network

**XUESONG ZHOU, YANGYANG CUI, AND YOUJIE MA**

Tianjin Key Laboratory for Control Theory & Applications in Complicated Industry Systems, School of Electrical and Electronic Engineering, Tianjin University of Technology, Tianjin 300384, China

Corresponding authors: Yangyang Cui (183121308@stud.tjut.edu.cn) and Xuesong Zhou (zxsmyj@126.com)

This work was supported in part by the National Natural Science Foundation of China under Grant 51877152, and in part by the Natural Science Foundation of Tianjin of China under Grant 18JCZDJC97300.

**ABSTRACT** In order to reduce the capacity of the active power filter (APF), improve its dynamic tracking speed and anti-disturbance ability of harmonic currents, so as to better solve the problem of harmonic pollution in the medium and high voltage distribution network, this article is suitable for medium and high voltage distribution networks. The three-phase three-wire injection hybrid active power filter (IHAPF) of high voltage distribution network is the research object, and a fuzzy linear active disturbance rejection controller (Fuzzy-LADRC) suitable for IHAPF voltage outer loop control is proposed. The controller is composed of a fuzzy proportional controller, a linear extended state observer (LESO), and a total disturbance compensation link. The introduction of fuzzy logic control solves the difficult problem of controller parameter tuning, and uses Lyapunov stability definition to prove the stability of the system. Finally, the control performance of IHAPF under the control of Fuzzy-LADRC is simulated and verified by MATLAB&SIMULINK simulation platform, and compared with the traditional PI controller. The results show that the Fuzzy-LADRC controller is better than the traditional PI controller and has good tracking and anti-disturbance capabilities.

**INDEX TERMS** Injection hybrid active power filter (IHAPF), linear active disturbance rejection controller (LADRC), fuzzy control, voltage outer loop, stability, anti-disturbance characteristics.

## I. INTRODUCTION

With the development of science technology and the increasing demand for electricity, a large number of power electronic equipment and various non-linear loads have been invested in the power grid. Voltage fluctuations, flicker, three-phase unbalance and current waveform distortion have become the focus of attention. Among them, the problem of harmonic pollution is the most serious, which has caused a serious decline in power quality of the power grid [1]–[3]. The APF with good compensation characteristics, strong suppression capability and fast dynamic response has become the main method of harmonic control [4]–[6]. Due to the increase in the capacity of switching devices, the APF capacity can meet the requirements of low voltage occasions. However, in the medium and high voltage large capacity system, the traditional series and parallel structure APF can't meet the harmonic suppression requirements [7]. Due to the function of the injection branch, IHAPF makes the fundamental voltage only act on the injection branch, and the active part only bears the harmonic voltage, so it has the ability to provide reactive power compensation and harmonic suppression in the medium and high voltage distribution system.

At present, people's research on IHAPF is mainly based on the double closed-loop control strategy of the traditional PI controller [8]. The harmonic component of the load current is detected by the harmonic current detection method, and then harmonic currents of equal magnitude and opposite direction are injected into the grid to achieve the purpose of compensation. However, the traditional PI control algorithm cannot solve the contradiction between the "tracking" and "disturbance resistance" of the system, showing huge limitations. This control method cannot suppress the passive filter of the grid series and parallel resonance problems. It will also cause

The associate editor coordinating the review of this manuscript and approving it for publication was Zhixiang Zou.

system instability and slow response speed [9]–[11]. Linear active disturbance rejection controller (LADRC) is proposed in the process of continuous in-depth thinking on the inner thoughts of traditional PID controllers and modern control theory [12], [13]. It does not depend on the mathematical model of the controlled object and can effectively perform the overall disturbance of the entire system. Compensation is estimated to be accurate, and LADRC also has a natural decoupling [14]. Reference [15] uses LADRC for shunt hybrid active power filter (SHAPF) double closed-loop control, which greatly improves its control performance. Therefore, the current tracking control link of IHAPF based on the LADRC controller can quickly track the changes of harmonic currents in the medium and high voltage distribution network. When the system is subject to large disturbances, LESO can effectively estimate and compensate it, so that the system based on LADRC controller control has strong robustness and adaptability. In medium and high-voltage high-power inverters, switching devices usually work at lower switching frequencies to reduce losses, but this will cause severe current distortions, increased harmonics, and even instability, so that the inverter cannot work normally. The use of LADRC strategy can estimate and compensate its impact as the total disturbance. However, whether a controller can obtain satisfactory control performance depends on whether its parameters can be adjusted properly. Due to the difficulty of LADRC parameter tuning, it is difficult to exert its unique control performance. References [13] and [16] proposed a parameter tuning rule for active disturbance rejection controller based on ant colony algorithm and particle swarm optimization. These methods successfully applied to the frequency conversion speed regulation of permanent magnet synchronous motor, which greatly improves the control effect. The reference [17] combines fuzzy control with PID controller and uses it in the APF current tracking control link, which improves the efficiency of parameter tuning. Because fuzzy control is difficult to obtain the mathematical model, it is very suitable for the objects whose dynamic characteristics are difficult to master or change very significantly, especially for the control of nonlinear, time-varying and pure lag systems. In addition, such as synovial control and droop control are gradually being used in the APF control system.

In conclusion, due to the mutual coupling between the voltage outer loop and the current inner loop of the IHAPF double closed-loop control system, in order to better solve the harmonic pollution problem in the medium and high voltage distribution network. This paper proposes a suitable Fuzzy-LADRC controller with IHAPF voltage outer loop. The controller combines the advantages of fuzzy logic control parameter adaptive adjustment and LADRC total disturbance compensation, and can eliminate various problems caused by parameter setting and system uncertainty disturbance. Since the Lyapunov stability proof method is not only suitable for linear systems but also for the proof of the stability of nonlinear systems. This paper uses the Lyapunov stability definition to analyze the stability of the IHAPF voltage outer loop based on the Fuzzy-LADRC controller. Finally, simulation experiments verify the correctness and effectiveness of the control method proposed in this article.

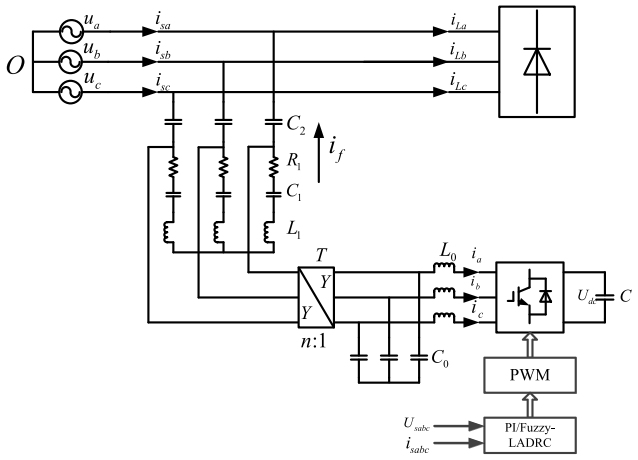


**FIGURE 1.** IHAPF main circuit system structure diagram.

## II. MATHEMATICAL MODEL OF IHAPF

Figure 1 shows the IHAPF main circuit structure diagram, where $u_a$, $u_b$ and $u_c$ are three-phase grid voltage; $i_{sa}$, $i_{sb}$ and $i_{sc}$ are three-phase grid current; $i_f$ is the compensation current output by the filter; $C_0$ and $L_0$ are PWM respectively the filter capacitor and filter inductance of the converter; $C$ is the DC side capacitor; $U_{dc}$ is the DC side voltage, $T$ is the coupling transformer, and $n$ is the transformation ratio of the coupling transformer. The passive part mainly includes the fundamental series resonant branch composed of $R_1, L_1, C_1$ and the injection capacitor $C_2$ [18].

It can be seen from the structure diagram that the entire IHAPF runs in parallel with the power grid and is mainly composed of active filtering and passive filtering. The basic operating principle is: the fundamental series resonant branch formed by $C_1$ and $L_1$ has series resonance at the fundamental frequency. The fundamental impedance of this branch is approximately zero, and the fundamental voltage will be added to the injection both ends of capacitor $C_2$. Since the harmonic impedance of the fundamental series resonant branch is proportional to the frequency, the harmonic impedance of the injected capacitor $C_2$ is inversely proportional to the frequency. Therefore, as the frequency increases, the harmonic impedance of the fundamental series resonant branch will increase, and the harmonic impedance of the injection capacitor $C_2$ will be reduced. At this time, the harmonic voltage is mainly applied to both ends of the fundamental series resonant branch, thereby reducing the voltage added to the PWM converter and effectively reducing the capacity of the filter [19]. This feature ensures that IHAPF can be applied to medium and high voltage power distribution systems.

According to the system structure diagram shown in Figure 1, the single phase equivalent circuit is shown in Figure 2.

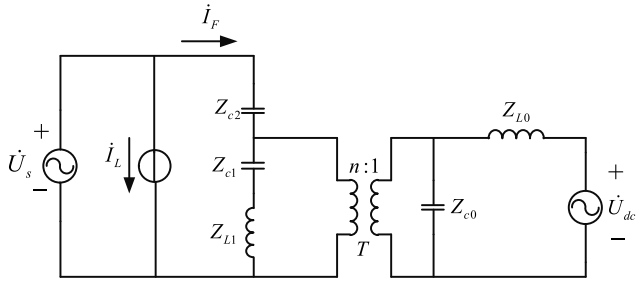


**FIGURE 2.** IHAPF single phase equivalent circuit.

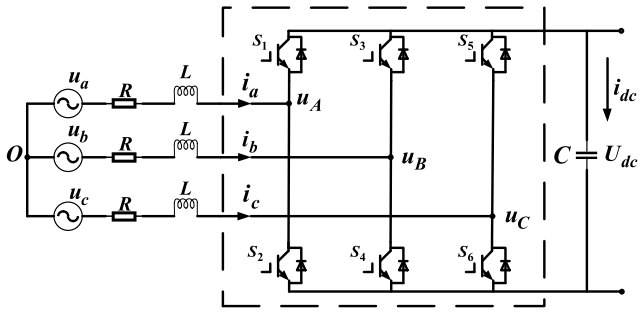


**FIGURE 3.** IHAPF switch circuit structure diagram.

From Figure 2 the equivalent parameters of the system are:

$$L = \frac{1}{\omega}\mathrm{Im}\,(Z) = \frac{1}{\omega}\mathrm{Im}\left\{Z_{L0} + \left[Z_{C0}//\left(\frac{Z_{eq}}{n^2}\right)\right]\right\} \tag{1}$$

$$R = \mathrm{Re}\,(Z) = \mathrm{Re}\left\{Z_{L0} + \left[Z_{C0}//\left(\frac{Z_{eq}}{n^2}\right)\right]\right\} \tag{2}$$

Among them, $\omega$ is the system angular frequency; $Z_{L0}$ and $Z_{C0}$ are the impedances of the filter, inductance $L_0$ and the filter capacitor $C_0$ output by the filter, $Z_{eq}$ is the equivalent impedance seen from the secondary side of the transformer.

In order to establish its mathematical model, the system structure diagram shown in Figure 1 is equivalent to a switch circuit diagram, as shown in Figure 3:

In order to establish the mathematical model of IHAPF, let $S_j(j = A, B, C)$ be the switching function, and $S_j = 1$ means that the upper tube of the $j$-arm IGBT is on and the lower tube is off; the switching state represented by $S_j = 0$ is opposite to the switching state at $S_j = 1$. This ensures that each of the upper and lower bridge arms has an IGBT for conduction. $b_j w_j(j = a, b, c, u)$ represents the interference of IHAPF AC side and DC side switching loss, detection error, and external factors to the system.

From the switch function:

$$u_j = \left(S_j - \frac{1}{3}\sum_{j=A,B,C} S_j\right) U_{dc} \tag{3}$$

Assuming that the voltage and current of the three-phase power supply are symmetrical, the AC side equation of IHAPF can be obtained from Figure 3 as:

$$\begin{cases} L\dfrac{di_a}{dt} + Ri_a = u_a - \left(S_A - \dfrac{1}{3}\displaystyle\sum_{j=A,B,C} S_j\right) U_{dc} + b_a w_a \\ L\dfrac{di_b}{dt} + Ri_b = u_b - \left(S_B - \dfrac{1}{3}\displaystyle\sum_{j=A,B,C} S_j\right) U_{dc} + b_b w_b \\ L\dfrac{di_c}{dt} + Ri_c = u_c - \left(S_C - \dfrac{1}{3}\displaystyle\sum_{j=A,B,C} S_j\right) U_{dc} + b_c w_c \end{cases} \tag{4}$$

Then the DC side equation is:

$$C\frac{dU_{dc}}{dt} = S_A i_a + S_B i_b + S_C i_c + b_u w_u \tag{5}$$

Therefore, the IHAPF state space expression can be obtained as:

$$\dot{x} = Ax + Bu \tag{6}$$

Among them:

$$A = \begin{pmatrix} -\dfrac{R}{L} & 0 & 0 & -\dfrac{1}{L}\left(S_A - \dfrac{1}{3}\displaystyle\sum_{j=A,B,C} S_A\right) \\ 0 & -\dfrac{R}{L} & 0 & -\dfrac{1}{L}\left(S_B - \dfrac{1}{3}\displaystyle\sum_{j=A,B,C} S_B\right) \\ 0 & 0 & -\dfrac{R}{L} & -\dfrac{1}{L}\left(S_C - \dfrac{1}{3}\displaystyle\sum_{j=A,B,C} S_C\right) \\ \dfrac{S_A}{C} & \dfrac{S_B}{C} & \dfrac{S_C}{C} & 0 \end{pmatrix} \tag{7}$$

$$B = \begin{pmatrix} -\dfrac{1}{L} & 0 & 0 & \dfrac{b_a w_a}{L} \\ 0 & -\dfrac{1}{L} & 0 & \dfrac{b_b w_b}{L} \\ 0 & 0 & -\dfrac{1}{L} & \dfrac{b_c w_c}{L} \\ 0 & 0 & 0 & \dfrac{b_u w_u}{L} \end{pmatrix} \tag{8}$$

$$x = \begin{pmatrix} i_a & i_b & i_c & U_{dc} \end{pmatrix}^T \tag{9}$$

$$u = \begin{pmatrix} u_a & u_b & u_c & 1 \end{pmatrix}^T \tag{10}$$

In the IHAPF control system shown in Figure 1, the current inner loop and voltage outer loop double closed loop control mode are adopted, the voltage outer loop is controlled by fuzzy LADRC, and the current inner loop is controlled by hysteresis loop.

## III. DESIGN OF IHAPF VOLTAGE OUTER LOOP CONTROL SYSTEM BASED ON LADRC AND ANALYSIS OF ANTI-DISTURBANCE CHARACTERISTICS

### A. DESIGN OF IHAPF VOLTAGE OUTER LOOP CONTROL SYSTEM BASED ON LADRC

Traditional LADRC is composed of linear tracking differentiator (LTD), linear state error feedback control law (LSEF),

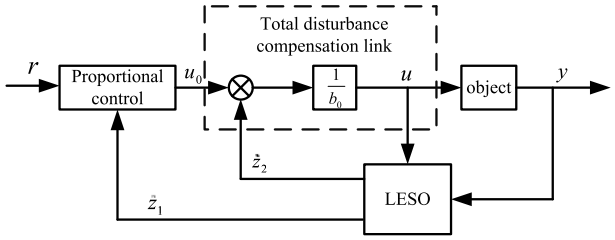


**FIGURE 4.** LADRC control block diagram.

linear extended state observer (LESO), and total disturbance compensation [20], [21]. The control block diagram is shown in Figure 4. Due to the relatively mature arrangement transition process in the current industrial control field and in order to avoid the system from generating high frequency oscillations, this article does not use LTD.

From equation (6), any phase of IHAPF is a first-order differential equation, so first-order LADRC (LESO is second-order) is used to control it. For the first-order system, since there is no observation of the differential of the state, LESO only estimates the two variables of the system. Therefore, LSEF only needs to adopt pure proportional control.

This article adopts the triangular wave comparison method in PWM tracking control technology to modulate the IHAPF pulse signal. The duty cycle of this modulation method is:

$$d_j = \frac{1}{2}\left(1 + \frac{v_j}{V_{ti}}\right) \quad (j = A, B, C) \tag{11}$$

In the formula, $V_{ti}$ is the amplitude of the triangular wave carrier; $v_j$ is the instantaneous value of the $j$-phase harmonic compensation current.

From equations (5) and (11), it can be obtained:

$$\dot{U}_{dc} = f_u + b_{u0}u_{u0} \tag{12}$$

In the formula, $f_u$ is the total disturbance, $b_{u0}$ is the control gain, and:

$$b_{u0} = \frac{1}{2CV_{ti}} \tag{13}$$

Let $x_1 = U_{dc}$ and $x_2 = f_u$. Combining (5) and (12) together and transforming them into a continuous expanded state space is:

$$\begin{cases} \dot{x} = Ax + Bu + E\dot{f} \\ y = Cx \end{cases} \tag{14}$$

Among them:

$$A = \begin{pmatrix} 0 & 1 \\ 0 & 0 \end{pmatrix}, \quad B = \begin{pmatrix} b_0 \\ 0 \end{pmatrix}, \quad C = \begin{pmatrix} 1 & 0 \end{pmatrix}, \quad E = \begin{pmatrix} 0 \\ 1 \end{pmatrix} \tag{15}$$

where $y$ is the output of the system.

The corresponding LESO is:

$$\begin{cases} \dot{z} = Az + Bu + H\left(y - \hat{y}\right) \\ \hat{y} = Cz \end{cases} \tag{16}$$

Among them, $z$ is the state vector of the observer, $H$ is the observer error feedback gain matrix, and:

$$H = \begin{pmatrix} \beta_1 \\ \beta_2 \end{pmatrix} \tag{17}$$

For the first-order system, LSEF adopts pure proportional control. From the above analysis, the IHAPF voltage outer loop control model based on traditional LADRC can be shown in equations (18), (19) and (20):

$$\begin{cases} \dot{z}_1 = z_2 - \beta_{u1}\left(z_1 - U_{dc}\right) + b_{u0}u_u \\ \dot{z}_2 = -\beta_{u2}\left(z_1 - U_{dc}\right) \end{cases} \tag{18}$$

$$u_{u0} = k_{up}\left(U_{ref} - z_1\right) \tag{19}$$

$$u_u = \frac{u_{u0} - z_2}{b_{u0}} \tag{20}$$

In the formula, $z_1$ and $z_2$ are the state estimates of $x_1$ and $x_2$. (19), (20) are the control models of LSEF and total disturbance compensation link respectively.

According to the performance requirements of the control system, all observer poles are configured at the observer bandwidth, and the controller poles are configured at the controller bandwidth, namely:

$$\begin{cases} s^2 + \beta_{u1}s + \beta_{u2} = (s + \omega_o)^2 \\ s + k_{up} = s + \omega_c \end{cases} \tag{21}$$

Then:

$$\begin{cases} \beta_{u1} = 2\omega_o \\ \beta_{u2} = \omega_o^2 \\ k_{up} = \omega_c \end{cases} \tag{22}$$

Among them, $\omega_c$ is the controller bandwidth, and $\omega_o$ is the observer bandwidth.

### B. ANTI-DISTURBANCE CHARACTERISTICS ANALYSIS

The core problem of the control system is stability, and its essence is anti-disturbance. The reference [22] uses frequency domain analysis to give the control based on traditional LADRC from two aspects: the control input gain uncertainty and the model parameter uncertainty. The stability analysis process of the current tracking control link of the three-phase four-wire shunt active power filter (SAPF) of the converter. This method is also suitable for the stability of the IHAPF voltage outer loop based on the traditional LADRC controller.

As the tracking and anti-disturbance of the evaluation system's anti-disturbance ability, for the PID controller, the tracking and anti-disturbance are reversed, and LADRC can well solve the contradiction between the tracking and anti-disturbance. This section uses the frequency domain analysis method to analyze the anti-interference characteristics of the IHAPF voltage outer loop based on the traditional LADRC.

Converting equations (18), (19), (20) into transfer functions and substituting them into equation (22) can be

obtained:

$$\begin{cases} Z_1(s) = \dfrac{\omega_o^2 + 2\omega_o s}{(s+\omega_o)^2} Y(s) + \dfrac{b_{u0} s}{(s+\omega_o)^2} U_u(s) \\ Z_2(s) = \dfrac{\omega_o^2 s}{(s+\omega_o)^2} Y(s) - \dfrac{b_{u0}\omega_o^2}{(s+\omega_o)^2} U_u(s) \\ U_u(s) = \dfrac{1}{b_{u0}} \left[\omega_c U_{ref}(s) - \omega_c Z_1(s) - Z_2(s)\right] \end{cases} \tag{23}$$

Further simplification can be obtained:

$$U_u(s) = \frac{1}{b_{u0}} \frac{(s+\omega_o)^2}{(s+\omega_o)^2 + \omega_c s - \omega_o^2} \left[ \omega_c U_{ref}(s) - \frac{\left(2\omega_c\omega_o + \omega_o^2\right) + \omega_c\omega_o^2}{(s+\omega_o)^2} Y(s) \right] \tag{24}$$

Order:

$$\begin{cases} G_1(s) = \dfrac{(s+\omega_o)^2}{(s+\omega_o)^2 + \omega_c s - \omega_o^2} \\ H_1(s) = \dfrac{\left(2\omega_c\omega_o + \omega_o^2\right) + \omega_c\omega_o^2}{(s+\omega_o)^2} \end{cases} \tag{25}$$

From $f_u = \dot{U}_{dc} - b_{u0}u_u = \dot{y} - b_{u0}u_u$, it can be concluded that:

$$F_u(s) = sY(s) - b_{u0}U_u(s) \tag{26}$$

From equations (24) and (26), it can be concluded that:

$$Y(s) = \frac{1}{s}F_u(s) + \frac{1}{s}\omega_c U_{ref}(s) G_1(s) - \frac{1}{s}Y(s) H(s) G_1(s) \tag{27}$$

By substituting formula (25) into equation (27) and simplifying it, it can be concluded that:

$$Y(s) = \frac{s^2 + (2\omega_o + \omega_c)s}{(s+\omega_c)(s+\omega_o)^2} F_u(s) + \frac{\omega_c}{s+\omega_c} U_{ref}(s) \tag{28}$$

From equation (28), the transfer function of the disturbance term is:

$$\delta(s) = \frac{Y(s)}{F_u(s)} = \frac{s^2 + (2\omega_o + \omega_c)s}{(s+\omega_c)(s+\omega_o)^2} \tag{29}$$

From equation (29), it can be concluded that the disturbance term of the three-phase four-wire IHAPF voltage outer loop control system under the control of the LADRC is only related to $\omega_o$ and $\omega_c$. Let $\omega_o = 10$ and $\omega_c$ take 10(rad/s), 20(rad/s), 30(rad/s), and 40(rad/s) respectively, the Bode diagram of the disturbance term of the control system can be obtained as shown in Figure 5(a). Let $\omega_c = 10$ and $\omega_o$ take 10(rad/s), 20(rad/s), 30(rad/s), and 40(rad/s), then the Bode diagram of the disturbance term of the control system is shown in Figure 5(b). When $\omega_c$ and $\omega_o$ take 10(rad/s), 100(rad/s), 1000(rad/s) and 10000 (rad/s) at the same time, it can get the Bode diagram of the disturbance term of the control system is shown in Figure 5(c).

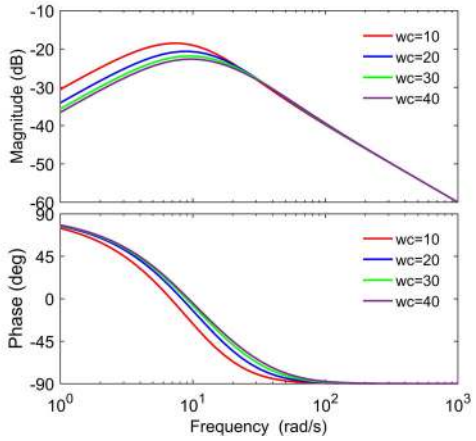


(a)

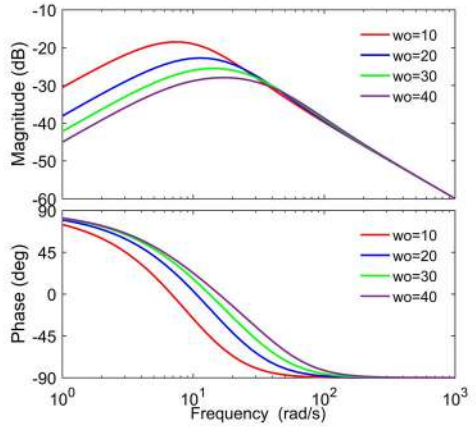


(b)

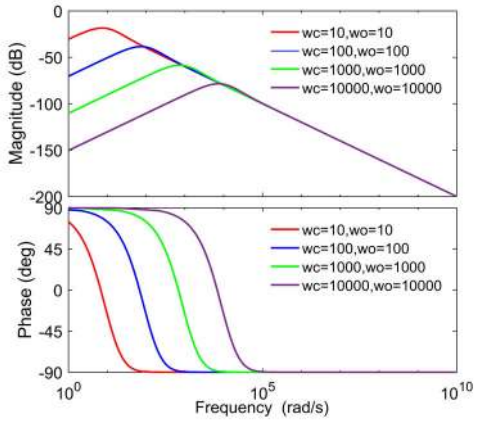


(c)

**FIGURE 5.** Perturbation term Bode diagram. (a) When $\omega_o$ remains unchanged; (b) When $\omega_c$ remains unchanged; (c) When changing $\omega_c$ and $\omega_o$ at the same time.

It can be seen from Figure 5 that adding $\omega_c$ and $\omega_o$ can increase the bandwidth of the system, enhance the anti-interference ability of the system, and also improve the tracking performance of the system.

Choosing disturbance $f_u$ as the unit step signal, the output response of the disturbance term can be obtained from equation (29):

$$Y(s) = \frac{s + 2\omega_o + \omega_c}{(s + \omega_c)(s + \omega_o)^2} = \frac{A}{(s + \omega_o)^2} + \frac{B}{s + \omega_o} + \frac{C}{s + \omega_c} \tag{30}$$

Among them:

$$\begin{cases} A = \dfrac{\omega_c + \omega_o}{\omega_c - \omega_o} \\ B = \dfrac{-2\omega_o}{(\omega_c - \omega_o)^2} \\ C = \dfrac{2\omega_o}{(\omega_o - \omega_c)^2} \end{cases} \tag{31}$$

The inverse Laplace transform of formula (30) and the limit value obtained are:

$$\lim_{t\to\infty} y(t) = \lim_{t\to\infty} \left(Ate^{-\omega_o t} + Be^{-\omega_o t} + Ce^{-\omega_c t}\right) = 0 \tag{32}$$

It can be concluded from equation (32) that the larger $\omega_c$ and $\omega_o$ are, the faster the attenuation of $y(t)$ is and the shorter the system recovery time.

## IV. DESIGN OF IHAPF VOLTAGE OUTER LOOP SYSTEM BASED On Fuzzy-LADRC

A lot of historical experience and engineering practice have shown that whether a controller can make the system obtain satisfactory control performance depends on whether its parameters are adjusted properly; for a general industrial controller, the difficulty is not the controller design and implementation of the controller is the parameter setting of the controller. As far as LADRC is concerned, it is necessary to tune the three parameters of controller bandwidth $\omega_c$, observer bandwidth $\omega_o$, and compensation factor $b_0$. The compensation factor $b_0$ represents the characteristics of the object and can be derived from the initial acceleration in the step response. For most engineering objects, the controller bandwidth $\omega_c$ and observer bandwidth $\omega_o$ can be adjusted by $\omega_o = (3 \sim 5)\,\omega_c$ . Therefore, the entire LADRC controller only needs to set the controller bandwidth $\omega_c$.

In conclusion, the parameter adaptive controller based on Fuzzy-LADRC proposed in this paper uses the error $e$, the error rate of change $\dot{e}$ and the fuzzy relationship between the parameters to adjust the LADRC controller parameters $\omega_c$. This method makes parameter tuning easier and has good control effects.

### A. Fuzzy-LADRC CONTROLLER DESIGN

Fuzzy control is the application of fuzzy theory in control engineering. It is a control system with the ability to simulate human learning and self-adaptation. Fuzzy control system is composed of four parts: fuzzy rules, fuzzification, fuzzy inference, and precise calculation [23], [24]. The schematic diagram of the control system is shown in Figure 6.

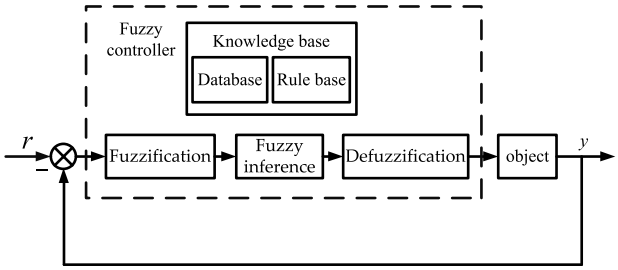


**FIGURE 6.** Fuzzy controller structure.

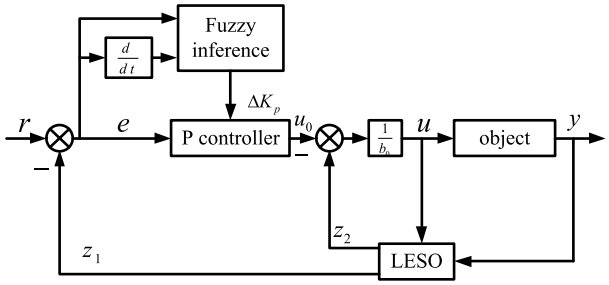


**FIGURE 7.** Fuzzy-LADRC controller structure diagram.

Since fuzzy control does not need to establish an accurate mathematical model of the controlled object, it can solve various uncertain problems in the system. However, its fuzzy processing of system information reduces the control performance and dynamic quality of the entire system. At the same time, when there is a large disturbance in the system, the fuzzy control does not have the ability to resist disturbance.

Combining the advantages of fuzzy control and LADRC, Fuzzy-LADRC is composed of three parts: fuzzy proportional controller, LESO and total disturbance compensation. It takes the error $e$ and the error change rate $\dot{e}$ between the input and output of the system as input, and the proportional coefficient increment $\Delta K_{up}$ as output. The controller parameters are modified according to the changes of $e$ and $\dot{e}$, which can be obtained:

$$K_{up_i} = K_{up_{i-1}} + \Delta K_{up} \quad (i = 1, 2, 3\cdots) \tag{33}$$

From the above analysis, the structure diagram of the Fuzzy-LADRC controller is shown in Figure 7.

Therefore, the IHAPF electric voltage outer loop control structure diagram based on Fuzzy-LADRC is shown in Figure 8 (a) and Figure 8(b) shows the current inner loop. Its control method adopts current hysteresis control. This control method does not require a carrier, the control method is easy to implement, and its current response is rapid, which can achieve rapid compensation of grid harmonic currents. The entire IHAPF control system formed by this is a double closed-loop control, which has strong stable performance.

The error $e$ between the compensation current output by IHAPF and the harmonic current of the system and its derivative $\dot{e}$ are taken as the input variable of the fuzzy logic controller, and $\Delta K_{up}$ is taken as the output variable. Their variation range is defined as the basic domain of fuzzy sets.

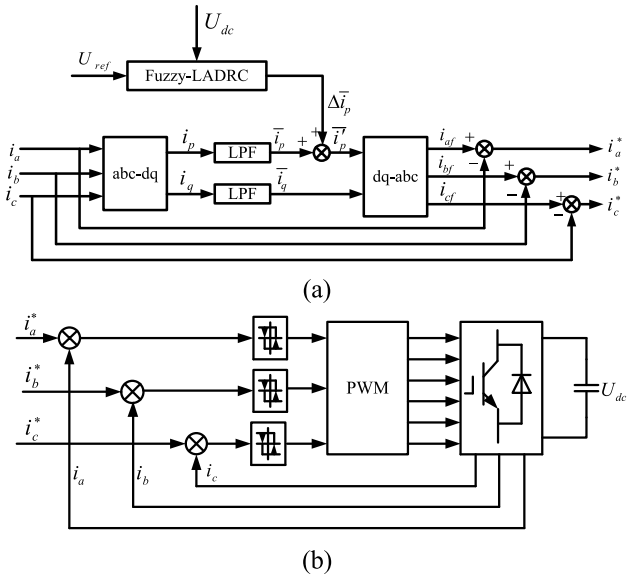


**FIGURE 8.** IHAPF double closed-loop control: (a) Voltage outer loop control structure diagram; (b) Current inner loop control structure diagram.

**TABLE 1.** Fuzzy control rule table.

| $\Delta K_p$ | | $e$ | | | | | | |
|---|---|---|---|---|---|---|---|---|
| | | **NB** | **NM** | **NS** | **ZO** | **PS** | **PM** | **PB** |
| $\dot{e}$ | **NB** | PB | PB | PM | PM | PS | ZO | ZO |
| | **NM** | PB | PB | PM | PS | PS | ZO | NS |
| | **NS** | PM | PM | PM | PS | ZO | NS | NS |
| | **ZO** | PM | PM | PS | ZO | NS | NM | NM |
| | **PS** | PS | PS | ZO | NS | NS | NM | NM |
| | **PM** | PS | ZO | NS | NM | NM | NM | NB |
| | **PB** | ZO | ZO | NM | NM | NM | NB | NB |

The basic domain of two inputs $e$ and $\dot{e}$ is $[-5,5]$, and the basic domain of output is $[-0.4,0.4]$. Take the fuzzy set {NB, NM, NS, ZO, PS, PM, PB}, and the elements in the subset represent negative large, negative medium, negative small, zero, positive small, positive middle, and positive large. The value of $e$ and $\dot{e}$ can be restricted within the specified range through formula (34).

$$y = \frac{6}{b-a}\left(x - \frac{a+b}{2}\right) \tag{34}$$

According to engineering practice experience, the fuzzy control rule table can be obtained as shown in Table 1:

According to the fuzzy rule table, the membership function of the input and output of the fuzzy control and the output surface are shown in Figure 9.

### *B. STABILITY ANALYSIS OF Fuzzy-LADRC*

The three main performances of the control system are stability, anti-disturbance and tracking. The primary purpose of the control system is to make the system operate stably

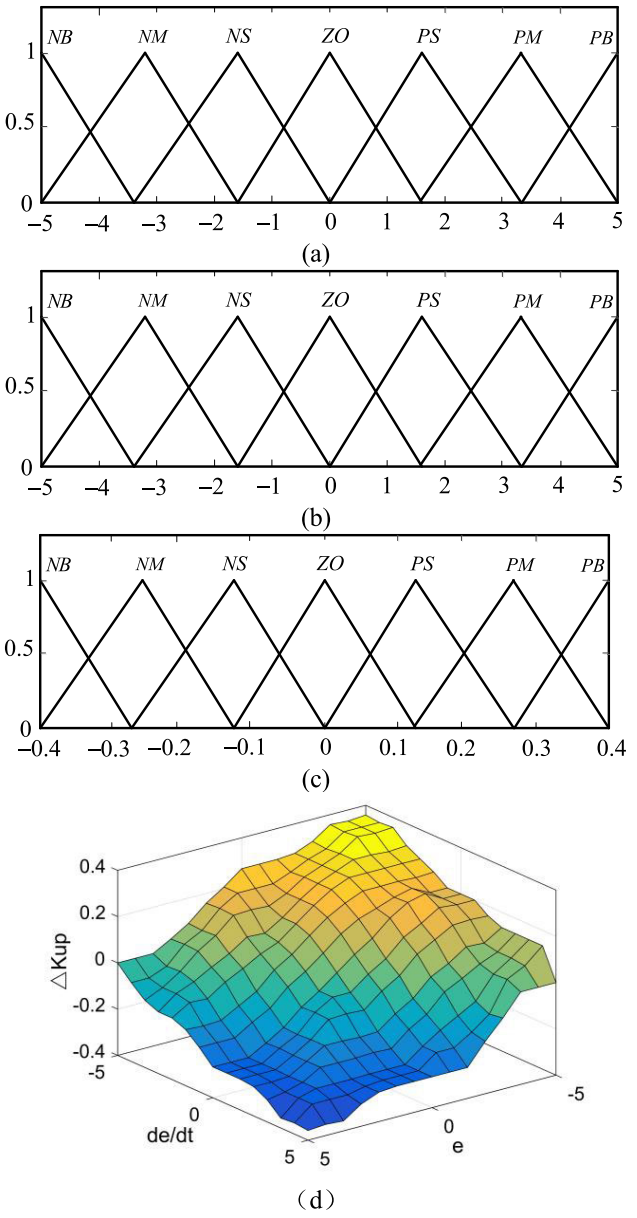


**FIGURE 9.** Fuzzy control input and output membership function and output surface: (a) Membership function of fuzzy control input error *e*; (b) Membership function of fuzzy control input error *e* rate of change; (c) Membership function of fuzzy control output; (d) Output surface of fuzzy controller $\Delta K_{up}$.

without being affected by undesired factors, or to be corrected in time after being affected, so that the system can remain in the desired state. The biggest advantage of the Fuzzy-LADRC controller proposed in this paper is that it utilizes the parameter adaptive principle of fuzzy control, and the topology of the LADRC controller itself has not undergone substantial changes, so the definition of Lyapunov stability can be used to the stability of the IHAPF voltage outer loop control link based on Fuzzy-LADRC is analyzed.

From equations (14) and (18), the LESO expression can be written as:

$$\begin{cases} \dot{z}_1 = z_2 + \beta_{u1}(x_1 - z_1) + b_{u0}u_u \\ \dot{z}_2 = \beta_{u2}(x_1 - z_1) + h(z, w) \end{cases} \tag{35}$$

From (17) and (22),it can be obtained:

$$H = \begin{pmatrix} \beta_{u1} \\ \beta_{u2} \end{pmatrix} = \begin{pmatrix} a_1\omega_o \\ a_2\omega_o^2 \end{pmatrix} = \begin{pmatrix} 2\omega_o \\ \omega_o^2 \end{pmatrix} \tag{36}$$

Among them, $a_1 = 2, a_2 = 1$.

Let $\tilde{x} = x_i - z_i\,(i = 1, 2)$, from equations (14) and (35), the LESO estimation error can be:

$$\begin{cases} \dot{\tilde{x}}_1 = \tilde{x}_2 - 2\omega_o\tilde{x}_1 \\ \dot{\tilde{x}} = h(x, w) - h(z, w) - \omega_o^2\tilde{x}_1 \end{cases} \tag{37}$$

Set $\varepsilon_i = \frac{\tilde{x}_i}{\omega_o^{i-1}}\,(i = 1, 2)$, then formula (37) can be changed to:

$$\begin{cases} \dot{\varepsilon}_1 = \omega_o\varepsilon_2 - 2\omega_o\varepsilon_1 \\ \dot{\varepsilon}_2 = -\omega_o\varepsilon_1 + \dfrac{h(x, w) - h(z, w)}{\omega_o} \end{cases} \tag{38}$$

Convert formula (38) into matrix form as:

$$\dot{\varepsilon}_i = \omega_o A_0 \begin{pmatrix} \varepsilon_1 \\ \varepsilon_2 \end{pmatrix} + B_0\frac{h(x, w) - h(z, w)}{\omega_o} \tag{39}$$

Among them:

$$A_0 = \begin{pmatrix} -2 & 1 \\ -1 & 0 \end{pmatrix} = \begin{pmatrix} -a_1 & 1 \\ -a_2 & 0 \end{pmatrix}, \quad B_0 = \begin{pmatrix} 0 \\ 1 \end{pmatrix} \tag{40}$$

From equation (22) and the Hurwitz stability criterion, $yA_0$ is stable. Then from the definition of Lyapunov's asymptotic stability, there must be a positive definite symmetric matrix $P$ such that $A_0$ satisfies: $A_0^T P + PA_0 = -E$ (where $E$ is the identity matrix). Then:

$$P = \begin{pmatrix} \frac{1}{2} & -\frac{1}{2} \\ -\frac{1}{2} & \frac{3}{2} \end{pmatrix} \tag{41}$$

Define the Lyapunov function as $v(\varepsilon) = \varepsilon^T P\varepsilon$, then:

$$\dot{v}(\varepsilon) = -\omega_o\left(\varepsilon_1^2 + \varepsilon_2^2\right) + \frac{h(x, w) - h(z, w)}{\omega_o}(-\varepsilon_1 + 3\varepsilon_2) \tag{42}$$

Since $h(x, w)$ satisfies the Lipschitz continuity condition in the domain, there is a constant $c$ such that:

$$|h(x, w) - h(z, w)| \le c\,\|x - z\| \tag{43}$$

Then:

$$\frac{|h(x, w) - h(z, w)|}{\omega_o}(-\varepsilon_1 + 3\varepsilon_2) \le c(-\varepsilon_1 + 3\varepsilon_2)\frac{\|x - z\|}{\omega_o} \tag{44}$$

The formula (44) can be changed from $-\varepsilon_1 + 3\varepsilon_2 = 2\varepsilon^T PB_0$ to:

$$2\varepsilon^T PB_0\frac{|h(x, w) - h(z, w)|}{\omega_o} \le 2\varepsilon^T PB_0 c\frac{\|x - z\|}{\omega_o} \tag{45}$$

When $\omega_0 \ge 1$, there are:

$$\frac{\|x - z\|}{\omega_o} = \frac{\|\tilde{x}\|}{\omega_o} \le \|\tilde{x}\| \tag{46}$$

From $\|PB_0c\| - 2\|PB_0c\| + 1 \ge 0$, it can be obtained:

$$2\varepsilon^T PB_0\frac{|h(x, w) - h(z, w)|}{\omega_o} \le \left(\|PB_0c\|^2 + 1\right)\|\varepsilon\|^2 \tag{47}$$

Then from equations (42) and (47):

$$\dot{v}(\varepsilon) \le -\omega_o\left(\varepsilon_1^2 + \varepsilon_2^2\right) + \left(\|PB_0c\|^2 + 1\right)\|\varepsilon\|^2 \tag{48}$$

When $\omega_o > \|PB_0c\|^2 + 1, \dot{v}(\varepsilon) < 0$, according to the definition of Lyapunov's asymptotic stability, it can be obtained:

$$\lim_{t\to\infty}\tilde{x}_i(t) = 0 \tag{49}$$

From equation (49), LESO is progressively stable.

Since the fuzzy adaptive control enables the LADRC controller parameter $k_{up} = \omega_c$ to be effectively adjusted, the equations (19), (20) and (23) can be obtained:

$$u_u = \frac{K_{upi}\left(U_{ref} - z_1\right) - z_2}{b_{u0}} \tag{50}$$

Set $e = U_{ref} - x_1$, then:

$$u_u = \frac{K_{upi}(e + \tilde{x}_1) - (x_2 - \tilde{x}_2)}{b_{u0}} \tag{51}$$

Further simplification can be obtained:

$$\dot{e} = -K_{upi}(e + \tilde{x}_1) - \tilde{x}_2 \tag{52}$$

The formula (40) is expressed as the state space form:

$$\dot{e}(t) = \left(-K_{upi}\right)e(t) + \begin{pmatrix} -K_{upi} & -1 \end{pmatrix}\begin{pmatrix} \tilde{x}_1(t) \\ \tilde{x}_2(t) \end{pmatrix} \tag{53}$$

According to a large number of reference documents and engineering practical experience, the controller parameters can be adjusted. The output change $K_{upi}$ of the fuzzy control is smaller than the initial value of the controller parameter $\Delta K_{up}$, so as to ensure $K_{up} > 0$. Therefore, $-K_{upi}$ makes the characteristic polynomial $\left(s - K_{upi}\right)$ satisfy the Routh criterion, so $\left(-K_{upi}\right)$ is Hurwitz stable.

From equation (51), it can be obtained:

$$\lim_{x\to\infty}\left\|\begin{pmatrix} -K_{upi} & -1 \end{pmatrix}\begin{pmatrix} \tilde{x}_1(t) \\ \tilde{x}_2(t) \end{pmatrix}\right\| = 0 \tag{54}$$

Then:

$$\lim_{x\to\infty}\|e(t)\| = 0 \tag{55}$$

According to the definition of Lyapunov's asymptotic stability and formulas (49) and (55), it can be concluded from the engineering point of view that the system under the control of Fuzzy- LADRC is stable.

**TABLE 2. System parameters.**

| Parameter | Value | Unit |
|---|---|---|
| Three-phase Grid Line Voltage | 35 | $kV$ |
| System Frequency | 50 | $Hz$ |
| DC Side Capacitor Voltage | 820 | $V$ |
| Filter Inductor | 1 | $mH$ |
| Filter Capacitor | 10 | $\mu F$ |
| Fundamental Series Resistance | 0.15 | $\Omega$ |
| Fundamental Series Inductance | 2.7 | $mH$ |
| Fundamental Series Capacitor | 1.9 | $\mu F$ |
| Injection Capacitor | 5 | $\mu F$ |

**TABLE 3. Controller parameters.**

| Parameter | Value |
|---|---|
| PI controller proportional adjustment coefficient | 4 |
| PI controller integral adjustment coefficient | 2 |
| Fuzzy-LADRC controller bandwidth initial value | 1000 |
| Fuzzy-LADRC observer bandwidth | 3000 |
| Fuzzy-LADRC compensation factor | 100000 |

## V. SIMULATION ANALYSIS

In order to verify the correctness and effectiveness of Fuzzy-LADRC, the MATLAB&SIMULINK simulation platform is used to simulate and verify the control system shown in Figure 1. Under the premise of the stability of the entire system, PI and Fuzzy-LADRC controllers are respectively used in the voltage outer loop control link of IHAPF. The three-phase uncontrollable rectifier is used as a nonlinear load. System parameters and controller parameters are shown in Table 2 and Table 3.

### A. TRACKING CHARACTERISTICS OF THE SYSTEM

Figure 10 is the waveform diagram and spectrum diagram of the three-phase load current before the system is compensated. It can be seen from the figure that when the system is not subjected to harmonic compensation, the three-phase load current waveform is seriously distorted, and the harmonic distortion rate is 22.94%.

In order to better compare and analyze the tracking ability of IHAPF under the control of Fuzzy-LADRC and PI on the harmonic currents in the medium and high voltage distribution network, this section takes the system phase A as an example to conduct a simulation analysis. Figure 11 shows the tracking effect of the harmonic current of the system under the control of PI and Fuzzy-LADRC.

It can be seen from Figure 11 (b) that under Fuzzy-LADRC control, the compensation current output by IHAPF can quickly track the change of system harmonic current, and the tracking error is approximately zero. However, when PI controller is used for control, there is still tracking error

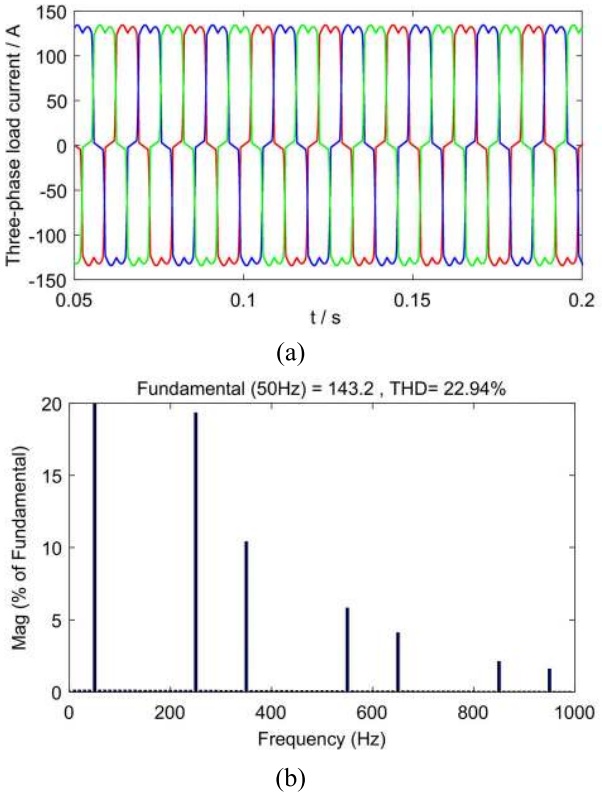


**FIGURE 10. Three-phase load current waveform and frequency spectrum: (a) Three-phase load current waveform; (b) Three-phase load current spectrum.**

between the waveform of harmonic compensation current and that of system harmonic current, as shown in Figure 11 (a). It is concluded that the speed of harmonic current tracking system output by IHAPF under PI control is relatively slow, which verifies that the dynamic tracking performance of Fuzzy-LADRC controller is better than that of PI controller.

Figure 12 shows the waveform and spectrum of three-phase grid current after compensation by PI and Fuzzy-LADRC controllers. It can be seen from the figure that the harmonic distortion rate of three-phase grid current after PI controller compensation is 4.21%, while that of three-phase power grid current compensated by Fuzzy-LADRC is 2.2%, which is far lower than that under PI control.

### B. ANTI-INTERFERENCE CHARACTERISTICS OF THE SYSTEM

In order to verify the anti-disturbance characteristics of the control strategy proposed in this paper, it is necessary not only to analyze the tracking and anti-disturbance characteristics of the AC side current, but also to analyze the stability of the DC side voltage, because the entire IHAPF control system is a double closed-loop control system. The current inner loop and the voltage outer loop have an interactive effect.

#### 1) ANALYSIS OF AC SIDE CURRENT TRACKING CONTROL

In order to verify the Fuzzy-LADRC controller has better anti-disturbance characteristics than the PI controller, the load

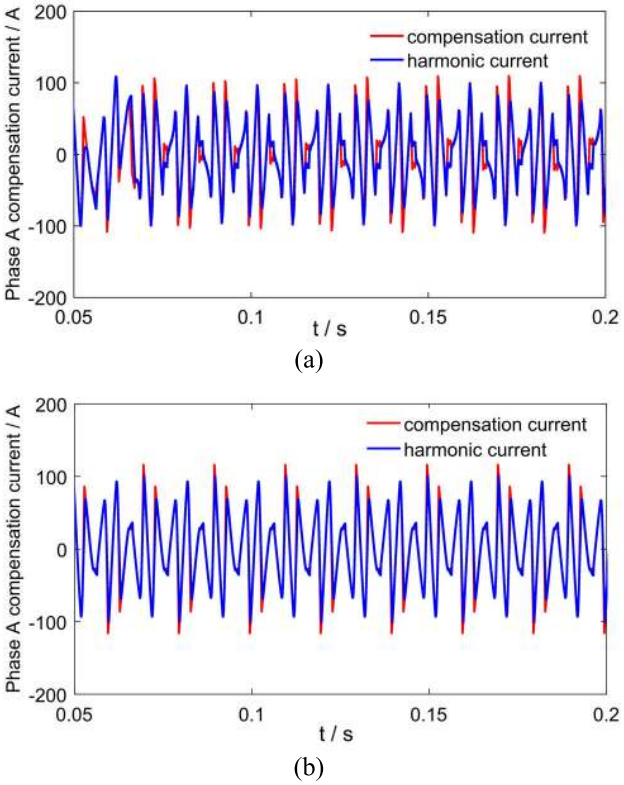


**FIGURE 11.** Phase A compensation current when controlled by different controllers: (a) Phase A compensation current when controlled by PI controller; (b) Phase A compensation current when controlled by Fuzzy-LADRC controller.

is switched on and off as a disturbance during the system operation. When it is set at 0.4s, the load is suddenly increased; at 0.6s, the load is suddenly removed. Then use Fuzzy-LADRC and PI controllers to track the changes of the system current, and then compare the changes of the grid-side current when it returns to the steady state. Figure 13 is the three-phase load-side current after switching the load. Figures 14(a) and 14(b) are the three-phase grid-side current after compensation using the Fuzzy-LADRC controller and the PI controller.

It can be seen from Figure 14(a) and Figure 14(b) that the system using Fuzzy-LADRC control has a fast current tracking speed when it returns to a steady state at 0.4s and 0.6s, and there is no transient process, and PI control is used when the system returns to a steady state, a short transient process occurs. It can be concluded that the system using Fuzzy-LADRC control will take less time to recover to the steady state after being disturbed by the outside than the PI controller, which verifies the Fuzzy-LADRC controller has better anti-disturbance than the PI controller.

### 2) DC SIDE VOLTAGE STABILITY ANALYSIS

Figure 15 is the change curve of the DC side voltage in the process of adding and subtracting the load. The reference input value of the DC side voltage is set to 820V. Figure (a)

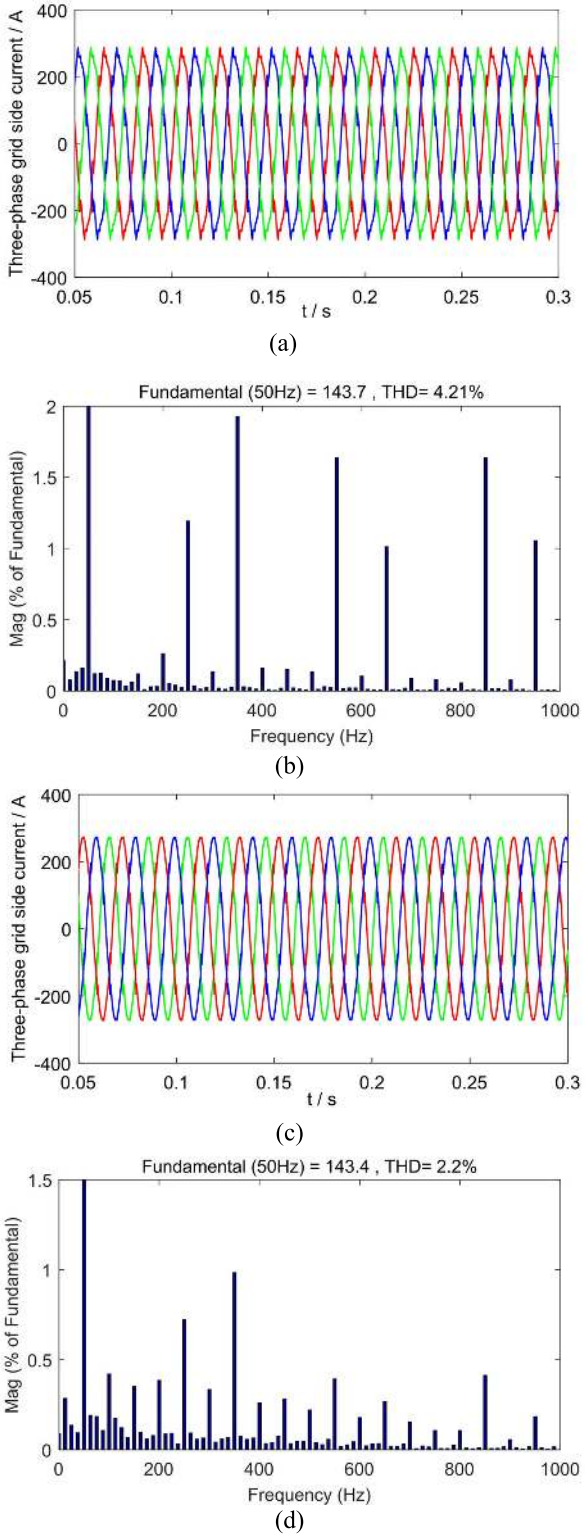


**FIGURE 12.** Waveform and spectrum diagram of three-phase grid current after compensation by different controllers: (a) Three-phase grid current waveform after compensation when controlled by PI controller; (b) Three-phase grid current spectrum after compensation when controlled by PI controller; (c) Three-phase grid current waveform after compensation when controlled by Fuzzy-LADRC controller; (d) Three-phase grid current spectrum after compensation when controlled by Fuzzy-LADRC controller.

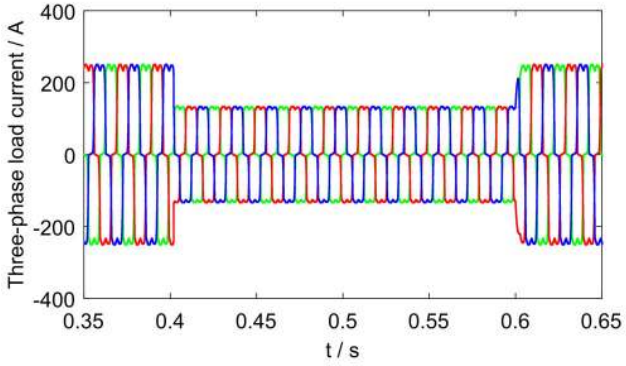


**FIGURE 13.** Three-phase load current waveform after load switching.

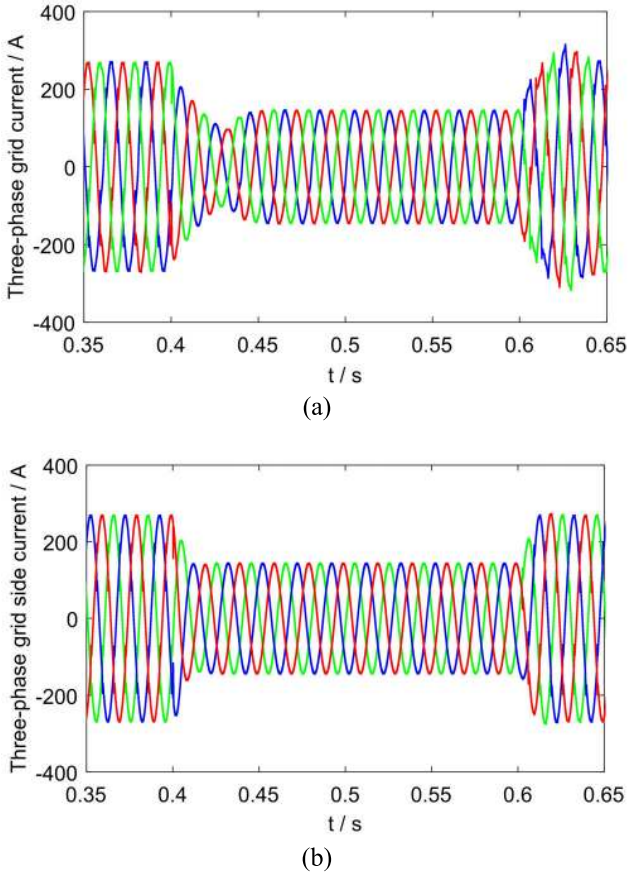


**FIGURE 14.** Waveform of three-phase grid current after compensation by different controllers: (a) Three-phase grid current waveform after compensation when controlled by PI controller; (b) Three-phase grid current waveform after compensation when controlled by Fuzzy-LADRC controller.

uses the PI controller and Figure (b) uses the Fuzzy-LADRC controller. To maintain the stability of the DC voltage measurement is to keep the capacitor voltage value of the PWM converter within the set value range. Because of the coupling between the voltage outer loop and the current inner loop, the control effect of the current inner loop will also have an effect on the voltage outer loop.

It can be seen from Figure 15 that when the system is loading and unloading, the DC side voltage of the system has an overshoot. When the load is increased, the peak value

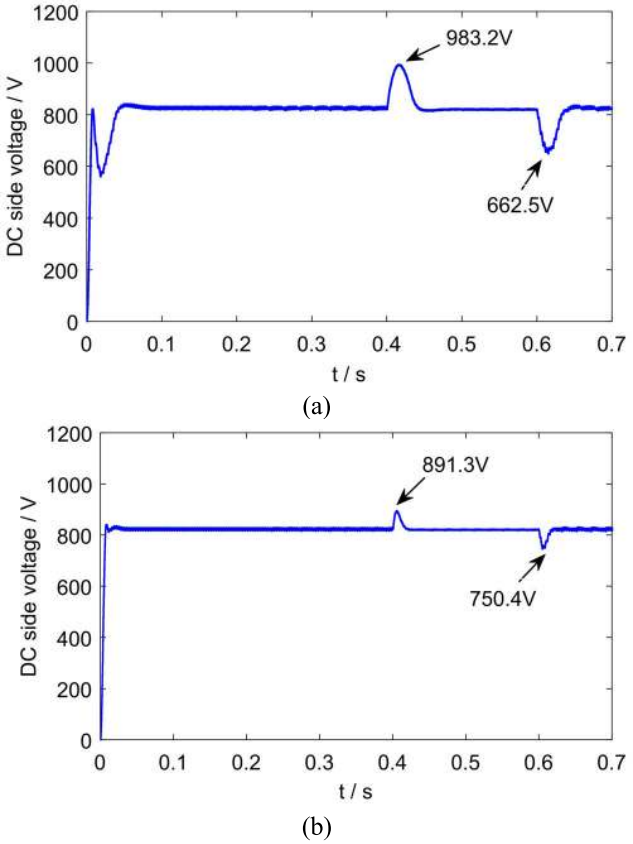


**FIGURE 15.** DC side voltage curve after using different controllers: (a) PI controller; (b) Fuzzy-LADRC controller.

of Figure (a) is 983.2V, and the peak value of Figure (b) is 891.3 V. When the load is subtracted, the peak value of figure (a) is 662.5V, and the peak value of figure (b) is 750.4V.

It can be seen from Figure (15) that the PI controller controlled system fluctuates at the initial moment, while the Fuzzy-LADRC controlled system reaches a stable value without fluctuations. It verifies the Fuzzy-LADRC controller has stronger anti-disturbance ability than the PI controller.

## VI. CONCLUSION

In order to reduce the capacity of the active power filter, the harmonics generated in the medium and high voltage distribution network are effectively controlled. Based on the operation mode of the medium and high voltage distribution network and the operating characteristics of IHAPF, this paper uses IHAPF, which is suitable for the medium and high voltage distribution network, as the compensation device, and establishes its mathematical model. On this basis, a first-order linear active disturbance rejection controller is designed and applied to the voltage outer loop control link, and the analysis process of disturbance rejection characteristics is given. In order to solve the difficult problem of controller parameter tuning, Fuzzy-LADRC with parameter self-tuning is proposed, and the stability of the control method is proved by the definition of Lyapunov stability. Finally, the tracking and anti-disturbance characteristics of IHAPF under the

control of Fuzzy-LADRC and PI are simulated and compared through MATLAB&SIMULINK simulation platform.

The results show that the disturbance rejection and tracking performance of the Fuzzy-LADRC controller are better than those of the traditional PI controller. Especially when there is a large disturbance in the system, the Fuzzy-LADRC can estimate and compensate the disturbance effectively, which overcomes the contradiction between "tracking" and" disturbance resistance " in the traditional PI controller. This control method has strong adaptability to environmental changes, and can automatically calibrate the linear active disturbance rejection controller in a random environment, so that the control system can still maintain a good performance even though when the characteristics of the controlled object are changed or disturbed.

## REFERENCES

[1] W. Feng, K. Sun, Y. Guan, J. M. Guerrero, and X. Xiao, "PCC voltage power quality restoring strategy based on the droop controlled grid-connecting microgrid," *J. Eng.*, vol. 2017, no. 13, pp. 1399–1403, Jan. 2017.
[2] S. Kan, X. Ruan, X. Huang, and H. Dang, "Second harmonic current reduction for flying capacitor clamped boost three-level converter in photovoltaic grid-connected inverter," *IEEE Trans. Power Electron.*, vol. 36, no. 2, pp. 1669–1679, Feb. 2021.
[3] J. S. Subjak and J. S. McQuilkin, "Harmonics-causes, effects, measurements, and analysis: An update," *IEEE Trans. Ind. Appl.*, vol. 26, no. 6, pp. 1034–1042, Nov./Dec. 1990.
[4] N. Xie, Q. Xu, J. Zeng, X. Liu, W. Zhang, and C. Zhang, "Noval hybrid control method for APF based on PI and FRC," *J. Eng.*, vol. 2019, no. 16, pp. 3002–3006, Mar. 2019.
[5] C. Xu, K. Dai, X. Chen, L. Peng, Y. Zhang, and Z. Dai, "Parallel resonance detection and selective compensation control for SAPF with square-wave current active injection," *IEEE Trans. Ind. Electron.*, vol. 64, no. 10, pp. 8066–8078, Oct. 2017.
[6] S. Rahmani, N. Mendalek, and K. Al-Haddad, "Experimental design of a nonlinear control technique for three-phase shunt active power filter," *IEEE Trans. Ind. Electron.*, vol. 57, no. 10, pp. 3364–3375, Oct. 2010.
[7] F. Ruixiang, L. An, and L. Xinran, "Parameter design and application research of shunt hybrid active power filter," *Proc. Chin. Soc. Elect. Eng.*, vol. 26, no. 2, pp. 106–111, Mar. 2006.
[8] A. A. Imam, R. S. Kumar, and Y. A. Al-Turki, "Modeling and simulation of a PI controlled shunt active power filter for power quality enhancement based on P-Q theory," *Electronics*, vol. 9, no. 4, pp. 3364–3375, Apr. 2020.
[9] G. Wang, R. Liu, N. Zhao, D. Ding, and D. G. Xu, "Enhanced linear ADRC strategy for HF pulse voltage signal injection-based sensorless IPMSM drives," *IEEE Trans. Power Electron.*, vol. 34, no. 1, pp. 514–525, Jan. 2019.
[10] A. Benrabah, D. Xu, and Z. Gao, "Active disturbance rejection control of *LCL*-filtered grid-connected inverter using Padé approximation," *IEEE Trans. Ind. Appl.*, vol. 54, no. 6, pp. 6179–6189, Nov./Dec. 2018.
[11] G. Wang, T. Li, G. Zhang, X. Gui, and D. Xu, "Position estimation error reduction using Recursive-Least-Square adaptive filter for model-based sensorless interior permanent-magnet synchronous motor drives," *IEEE Trans. Ind. Electron.*, vol. 61, no. 9, pp. 5115–5125, Sep. 2014.
[12] Z. Gao, "Scaling and bandwidth-parameterization based controller tuning," in *Proc. Amer. Control Conf.*, Denver, CO, USA, Jun. 2003, pp. 4989–4996.
[13] Z. Yin, C. Du, J. Liu, X. Sun, and Y. Zhong, "Research on autodisturbance-rejection control of induction motors based on an ant colony optimization algorithm," *IEEE Trans. Ind. Electron.*, vol. 65, no. 4, pp. 3077–3094, Apr. 2018.
[14] J. Han, *Active Disturbance Rejection Control Technology Control Technology for Estimating and Compensating Uncertain Factors*. Beijing, China: National Defense Industry Press, 2008.
[15] X. Zhou, C. Tian, Y. Ma, and J. Zhao, "Double closed-loop linear active disturbance rejection control of SHAPF," *Power Electron. Technol.*, vol.46, no. 3, pp. 1–3, 2012.
[16] C. Du, Z. Yin, Y. Zhang, J. Liu, Y. Zhong, X. Sun, and Y. Zhong, "Research on active disturbance rejection control with parameter autotune mechanism for induction motors based on adaptive particle swarm optimization algorithm with dynamic inertia weight," *IEEE Trans. Power Electron.*, vol. 34, no. 3, pp. 2841–2855, Mar. 2019.
[17] Y. Ma, F. Hong, X. Zhou, L. Tao, and X. Shi, "Controlling wind power grid connected converter based on differential tracker and fuzzy PID," *Mod. Electron. Technol.*, vol. 43, no. 17, pp. 96–101, 2020.
[18] J. Zhao, "Research on the application of active disturbance rejection control strategy in parallel hybrid active power filter," *Tianjin Univ. Technol.*, to be published.
[19] Z. Kong, X. Huang, Z. Wang, J. Xiong, and K. Zhang, "Active power decoupling for submodules of a modular multilevel converter," *IEEE Trans. Power Electron.*, vol. 33, no. 1, pp. 125–136, Jan. 2018.
[20] K. Liu, J. He, Z. Luo, X. Shen, X. Liu, and T. Lu, "Secondary frequency control of isolated microgrid based on LADRC," *IEEE Access*, vol. 7, pp. 53454–53462, 2019.
[21] G. Herbst, "A simulative study on active disturbance rejection control (ADRC) as a control tool for practitioners," *Electronics*, vol. 2, no. 4, pp. 246–279, Aug. 2013.
[22] X. Zhou, W. Liu, Y. Ma, J. Zhao, D. Wang, and Y. Qiu, "Analysis of three-phase four-wire shunt active power filter system based on LADRC," *High Voltage Technol.*, vol. 42, no. 4, pp. 1290–1299, 2016.
[23] Y. Ma, L. Tao, X. Zhou, W. Li, and X. Shi, "Analysis and control of wind power grid integration based on a permanent magnet synchronous generator using a fuzzy logic system with linear extended state observer," *Energies*, vol. 12, no. 15, p. 2862, Jul. 2019.
[24] P. J. Gaidhane, M. J. Nigam, A. Kumar, and P. M. Pradhan, "Design of interval type-2 fuzzy precompensated PID controller applied to two-DOF robotic manipulator with variable payload," *ISA Trans.*, vol. 89, pp. 169–185, Jun. 2019.

**XUESONG ZHOU** received the B.S. degree from the South China University of Technology, Guangzhou, China, in 1984, and the M.S. and Ph.D. degrees from Tsinghua University, Beijing, China, in 1990 and 1993, respectively. From 1993 to 2002, he worked with the School of Electrical and Automation Engineering, Qingdao University, as the Deputy Dean and Director of the Shandong Provincial Key Laboratory of Power Electronics Engineering. In 1997, he was promoted to a Full Professor at Qingdao University. Since 2002, he has been working with the School of Electrical and Electronic Engineering, Tianjin University of Technology, Tianjin, China. His research interests include power system analysis and automation, smart grid, and the field of new energy utilization.

**YANGYANG CUI** received the B.S. degree from the School of Electrical Engineering, Binzhou University, Binzhou, China, in 2018. He is currently pursuing the M.S. degree with the School of Electrical and Electronic Engineering, Tianjin University of Technology, Tianjin, China. His research interests include active disturbance rejection control technology and active power filter.

**YOUJIE MA** received the B.S., M.S., and Ph.D. degrees from Tsinghua University, Beijing, China, in 1987, 1990, and 1993, respectively. From 1993 to 2002, she worked with the School of Electrical and Automation Engineering, Qingdao University, where she was promoted to a Full Professor, in 1998. Since 2002, she has been working as a Distinguished Professor with the School of Electrical and Electronic Engineering, Tianjin University of Technology, Tianjin, China. Her research interests include power system analysis and automation and smart grid.